Plasmon-Assisted Selective and Super-Resolving Excitation of Individual Quantum Emitters on a Metal Nanowire

Qiang Li,[†,‡] Deng Pan,[§] Hong Wei,[*,†] and Hongxing Xu[§,‖]

[†]Institute of Physics, Chinese Academy of Sciences, Beijing 100190, China

[‡]Guangdong Provincial Key Laboratory of Nanophotonic Functional Materials and Devices, School of Information and Optoelectronic Science and Engineering, South China Normal University, Guangzhou 510006, China

[§]School of Physics and Technology, Wuhan University, Wuhan 430072, China

[‖]Institute for Advanced Studies, Wuhan University, Wuhan 430072, China

S Supporting Information

ABSTRACT: Hybrid systems composed of multiple quantum emitters coupled with plasmonic waveguides are promising building blocks for future integrated quantum nanophotonic circuits. The techniques that can super-resolve and selectively excite contiguous quantum emitters in a diffraction-limited area are of great importance for studying the plasmon-mediated interaction between quantum emitters and manipulating the single plasmon generation and propagation in plasmonic circuits. Here we show that multiple quantum dots coupled with a silver nanowire can be controllably excited by tuning the interference field of surface plasmons on the nanowire. Because of the period of the interference

pattern is much smaller than the diffraction limit, we demonstrate the selective excitation of two quantum dots separated by a distance as short as 100 nm. We also numerically demonstrate a new kind of super-resolution imaging method that combines the tunable surface plasmon interference pattern on the NW with the structured illumination microscopy technique. Our work provides a novel high-resolution optical excitation and imaging method for the coupled systems of multiple quantum emitters and plasmonic waveguides, which adds a new tool for studying and manipulating single quantum emitters and single plasmons for quantum plasmonic circuitry applications.

KEYWORDS: *Quantum dot, silver nanowire, surface plasmon, interference, optical super-resolution, structured illumination microscopy*
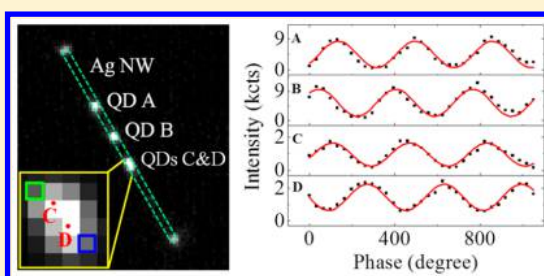
The ability to control the single photon emission from single solid state quantum emitters, such as semiconductor quantum dots (QDs) and color centers in nanodiamonds, is essential for various quantum information processing applications including quantum key distribution,[1] quantum networks,[2] and photonic quantum computing,[3] and so on. In recent years, various metal nanostructures supporting surface plasmon (SP) modes have been proposed to exquisitely tailor the photoluminescence properties of single quantum emitters,[4,5] realizing the enhanced excitation and emission rates,[6−9] and the directional radiation control.[10,11] In this context, the propagating SPs on metal nanowires (NWs) are particularly attractive due to their nanoscale field confinement and microscale propagation length[12−14] and hold promise for a wide range of applications in the fields such as enhanced light-matter interactions[15−17] and integrated nanophotonic circuits.[18−21] As a result of the potentially large Purcell effect, the propagating SP modes of the metal NW can efficiently harvest the photons emitted from single quantum emitters, resulting in an enhancement of the emitter's spontaneous decay rate as well as the generation of single SPs guided on the NW.[22−24] In the inverse process, a single propagating SP on the NW can be absorbed by an individual quantum emitter with

near unit probability.[25] The strong interaction between single quantum emitters and plasmonic NWs can be exploited to make integrated quantum optical devices such as efficient single-photon sources and transistors.[25−28]

In addition to single quantum emitters, the interaction of multiple quantum emitters mediated through the strong interaction with the SP modes on the plasmonic waveguide has been explored theoretically.[29−31] It has been reported that strong cooperative emission and high quantum entanglement between two quantum emitters can be achieved when the inter-emitter distance is of specific values.[32,33] However, there are challenges in experimentally studying the hybrid system of multiple quantum emitters coupled with the plasmonic waveguide. One is the super-resolution imaging of these quantum emitters along the waveguide. Although a recent experiment has demonstrated the imaging for two closely spaced QDs on a silver NW using the single molecule localization method,[34] for quantum emitters with temporally stabilized fluorescence, such as color centers,[35] multiple
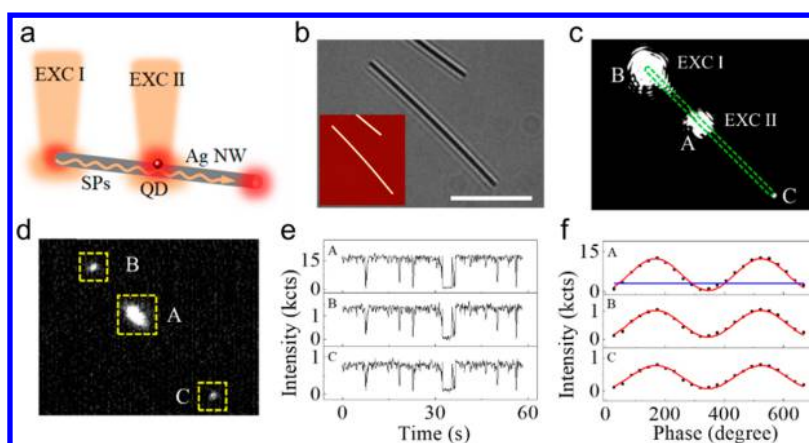
Figure 1. Modulating the excitation of a single QD by tuning the interference of propagating SPs and localized SPs on a Ag NW. (a) Sketch of exciting a QD-NW hybrid system by two coherent laser beams focused on one end of the NW (EXC I) and on the QD in the middle of the NW (EXC II). The generated propagating SPs are indicated by the wavy orange line. (b) Optical transmission image of the investigated QD-NW system. The inset shows the corresponding AFM image of the NW, revealing a NW diameter of 84 nm and a length of 12.8 μm. The scale bar corresponds to 5 μm. (c) Scattering image of the QD-NW system under the excitation shown in (a). The dashed green line shows the outline of the NW, and A, B, and C indicate the positions of the QD and the NW ends. (d) Fluorescence image of the same QD-NW system under the excitation of two laser beams. The bright spots at A, B, and C correspond to the radiative emission from the QD and the scattering of QD generated SPs at the two NW ends. The yellow squares denote the pixels used to track the intensities of the three bright spots. (e) Emission intensities of the spots A, B, and C as a function of time recorded at a rate of 10 frames per second. The intensity unit kcts stands for 1000 counts. (f) Emission intensities at A, B, and C under two-beam excitation with varying phase increment of the laser beam EXC I. The blue line indicates the emission intensity at A under absence of EXC II. The red lines represent sinusoidal fitting of the data.

quantum emitters in diffraction limited area cannot be resolved. Another challenge is to selectively control the excitation conditions of the quantum emitters in diffraction limited area, which cannot be achieved by using the conventional focused laser beam excitation method.[36−38]

The optical resolving and selective excitation of multiple quantum emitters near each other can be achieved by using the super-resolution methods, such as stimulated emission depletion (STED) technique, where the fluorescence emission process of the quantum emitters located away from the center of excitation spot is switched off through the depletion beam induced stimulated emission.[39−41] Yet, the existence of metal nanostructures strongly disturbs the field distribution of the excitation and depletion beams and reduces the resolution. Another state-of-the-art technique that may be employed for the super-resolution imaging and selective excitation of quantum emitters is scanning near-field optical microscopy with a nanofiber probe but the complexity and inflexibility of the technique limit its use in studying quantum emitters.[42,43] Because of these challenges, there is a high demand for a new kind of simple, flexible, and non-diffraction-limited optical resolving and excitation method for quantum emitters in plasmonic circuits.

In this paper, we first show that multiple QDs coupled with a Ag NW can be controllably excited by tuning the interference pattern of the localized and propagating SPs or two counter-propagating SP waves on the Ag NW. With this method, we demonstrated the selective excitation of two QDs separated by 100 nm, a distance much smaller than the diffraction limit. Finally, we numerically demonstrated a new kind of super-resolution imaging method by applying the tunable SP interference pattern on the NW to the structured illumination microscopy technique. Our finding points to a new way to excite and characterize multiple quantum emitters coupled with the plasmonic waveguide, which is essential for studying the plasmon mediated interaction between quantum emitters and

manipulating the generation and propagation of single SPs in the integrated quantum plasmonic circuit.

Figure 1a shows the sketch for the excitation of a single QD by using the interference field of propagating SPs and localized SPs on the Ag NW. The propagating SPs and localized SPs are generated by focusing two coherent laser beams, denoted as EXC I and EXC II, on one end and on the middle of the Ag NW, respectively. In experiment, for a Ag NW with a single CdSe/ZnS QD located at its near-field region (Figure 1b), two laser beams split from a 633 nm HeNe laser source were focused on the Ag NW (Figure 1c, see Section 1 of Supporting Information for more experimental details). In order to efficiently excite the propagating SPs and localized SPs, the polarization direction of the laser beam EXC I and EXC II were parallel and perpendicular to the NW, respectively.[44,45] The smaller bright spot at the NW end C (Figure 1c) indicates that the propagating SPs has been launched at the NW end B and coupled out as photons at the NW end C. The QD near the Ag NW can be either directly excited by the laser beam EXC II or remotely excited by the propagating SP field (see Section 2 of Supporting Information).[46] It is worth to mention that the Ag NW is coated by a 15 nm thick Al_2O_3 film to prevent the QD fluorescence quenching by the metal. The fluorescence image of the QD-NW system under the excitation of two laser beams (Figure 1d) shows three emission spots. The largest emission spot at A is the direct radiative emission from the QD. The time trace of the emission intensity from the QD (Figure 1e) shows a binary blinking behavior, that is, this emitter is randomly switched between ON (bright) and OFF (dark) states under continuous excitation, which is characteristic for single QD.[47] The two smaller spots at the NW ends B and C correspond to the scattering of the QD generated SPs at the NW ends, as demonstrated by the same blinking behavior as the QD fluorescence.

In order to tune the interference pattern of the propagating SPs and localized SPs on the NW, we controlled the phase
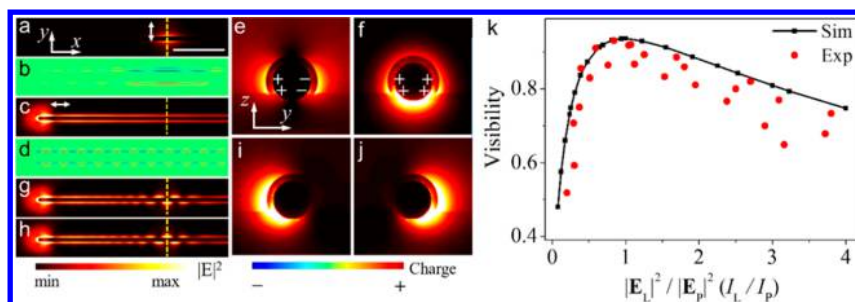
Figure 2. FDTD simulations of the interference of localized SPs and propagating SPs on a Ag NW. (a,c) Electric field intensity distributions of the NW at the plane 5 nm above the Al_2O_3 surface on glass substrate with polarized Gaussian beam focused on the middle (a) and the end (c) of the NW. The diameter of the Ag NW is 80 nm, and the Al_2O_3 thickness is 15 nm. The scale bar corresponds to 1 μm. The polarization direction of each beam is indicated by the white arrows. (b,d) Charge density distributions corresponding to (a,c). (e,f) Cross-sectional images of the electric field intensity distributions across the yellow dashed lines marked in (a,c). The surface charges are drawn schematically. The presumed QD position is 5 nm above the Al_2O_3 surface on glass substrate and 5 nm away from the Al_2O_3 surface on Ag NW (60 nm away from the center of the cross section of the Ag NW), where the electric field intensity of the localized SPs $|E_L|^2$ and propagating SPs $|E_P|^2$ are the same. (g,h) Electric field intensity distributions of the NW when two Gaussian beams illuminate the NW simultaneously. The phase difference of the two Gaussian beams is 0 (g) and π (h), respectively. (i,j) Cross-sectional images of the electric field intensity distributions across the yellow dashed lines marked in (g,h). (k) Simulated visibility of the interference of localized SPs and propagating SPs as a function of intensity ratio $|E_L|^2/|E_P|^2$ at the presumed QD position (black dots) and experimentally measured visibility of the QD emission intensity oscillation as a function of intensity ratio I_L/I_P for five QDs coupled with Ag NWs (red dots).

difference between the two excitation beams by using a Soleil-Babinet compensator. Figure 1f shows the emission intensities from the QD and the two NW ends as a function of the phase increment of the laser beam EXC I with the emission intensity of the QD under the excitation of only EXC I (I_P) and only EXC II (I_L) nearly the same ($I_L/I_P = 1.03$). Because of the different excitation efficiency of propagating SPs and localized SPs, here the intensity ratio of EXC I and EXC II is about 4.5 to produce similar QD emission intensity under single-beam excitation. The emission intensities of the QD and NW ends are found to be modulated with an oscillation of a period of 2π. The maximum value of the QD emission intensity I_{max} (12300 counts) is nearly four times as high as the intensity of the QD emission under single-beam excitation (I_P = 3200 counts, blue line in Figure 1f), and the minimum value of the QD emission intensity I_{min} is nearly zero. The visibility of the QD emission intensity oscillation is $(I_{max} - I_{min})/(I_{max} + I_{min})$ = 0.92, indicating the strong modulation of the electric field intensity on the NW resulting from the strong interference between propagating SPs and localized SPs.

To provide more insight and understanding of the phase-dependent modulation of the QD emission intensity, we performed electromagnetic calculations using a finite-difference time-domain (FDTD) method (FDTD Solutions). The NW is modeled as a cylinder which is semi-infinitely long and 80 nm in diameter. The refractive index of the Ag NW, glass substrate, and Al_2O_3 film at wavelength of 633 nm is set to be 0.05621 + 4.28107i,[48] 1.5 and 1.6, respectively. The top views (x−y plane) of the simulated electric field intensity and charge density distributions are shown in Figure 2a−d for focusing linearly polarized Gaussian beams of 633 nm wavelength on the middle and on the end of the NW. The cross-sectional (y−z plane) images of the electric field intensity distributions corresponding to the yellow dashed lines in Figure 2a,c are shown in Figure 2e,f, respectively. From the images it is evident that, both of the localized SPs and the propagating SPs have been generated and they are highly confined around the NW. The localized SPs give rise to an enhancement of the electric field intensity by a factor of 5.4 at the presumed position for the QD (5 nm away from the surfaces of Al_2O_3 on the substrate and on the NW)

compared with the case without NW, which will increase the excitation rate of the QD. For the localized SPs, the charges of opposite signs are transversely separated across the NW (Figure 2b). For the propagating SPs, the charge density shows a symmetric distribution in the y-direction (Figure 2d). Thus, the electric field of localized SPs and propagating SPs are antisymmetric and symmetric in the y-direction, respectively. Their superposition leads to an asymmetric field distribution in the y direction (one side is constructive interference and the other side is destructive interference). This is visible when the two SP modes are generated simultaneously (see Figure 2g,i). When traveling a distance of half a wavelength, the phase of the propagating SPs changes by π, so that the constructive interference area shifts to the opposite side of the NW, forming a zigzag shaped (periodically undulating) electric field intensity distribution at the overlap region of the two SP fields. With the phase of the propagating SPs changed continuously by tuning the initial phase of the excitation Gaussian beam at the NW end, the zigzag interference pattern moves along the NW. By a phase change of π for the propagating SPs, the positions with maximum and minimum field intensity exchange (Figure 2h,j, comparing to Figure 2g,i).

For the QD excited below the saturation condition, its emission intensity is proportional to the local electric field intensity. Under the two-beam excitation, the local electric field intensity at the QD position can be expressed as $|E_L|^2 + |E_P|^2 + 2E_L \cdot E_P \cos \Delta$, where E_L and E_P are the electric field of the localized SPs and propagating SPs, respectively, and Δ is the phase difference between them. The last term explains our experimentally observed phase dependent oscillation of QD emission intensity. In order to further verify the origin of the experimentally observed oscillatory emission intensity of the QD, we calculated the visibility of the phase-modulated electric field intensity at the presumed QD position under different electric field intensity ratio $|E_L|^2/|E_P|^2$ by varying the intensity of the Gaussian beam on the NW end (Figure 2k). Clearly, as the ratio deviates from unity, the visibility decreases. More calculation results show that changing the QD position has little influence on the visibility (see Section 3 of Supporting Information). The visibility of the experimental QD emission
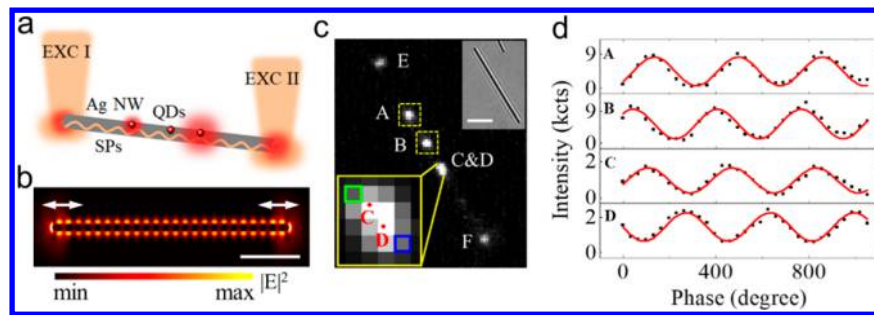
Figure 3. Controllable excitation of multiple QDs by shifting the SP standing wave along the NW. (a) Sketch of the controllable excitation of multiple QDs by using the SP standing wave generated by focusing two coherent laser beams on the two ends of a Ag NW. (b) Electric field intensity distribution of the NW at the plane 5 nm above the surface of Al_2O_3 on glass substrate with two linearly polarized Gaussian beams focused on the two ends of the NW. The diameter and length of the NW are 80 nm and 4 μm, respectively. The Al_2O_3 thickness is 15 nm. The polarization direction of each beam is indicated by the white arrows. The scale bar corresponds to 1 μm. From the interference pattern along the NW, the SP wavelength of λ_{SP} = 333 nm is obtained. (c) Fluorescence image of the investigated QDs-NW system under wide-field excitation. The bright spots A and B correspond to the fluorescence of two separated QDs A and B, while the elongated spot C&D corresponds to two QDs (QDs C and D) near each other. The spots E and F correspond to the two ends of the NW. The inset at the top right corner shows the optical transmission image of the Ag NW. The scale bar corresponds to 3 μm. The inset at the lower left corner is a magnified view of the spot C&D. The fitted positions of QDs C and D are marked with red dots. The yellow dotted, and the green and blue squares indicate the pixels used to track the intensities of QDs A and B, and C and D, respectively. (d) Emission intensities of the four QDs as a function of the phase increment of the laser beam EXC I. The red solid lines represent sinusoidal fitting of the data.
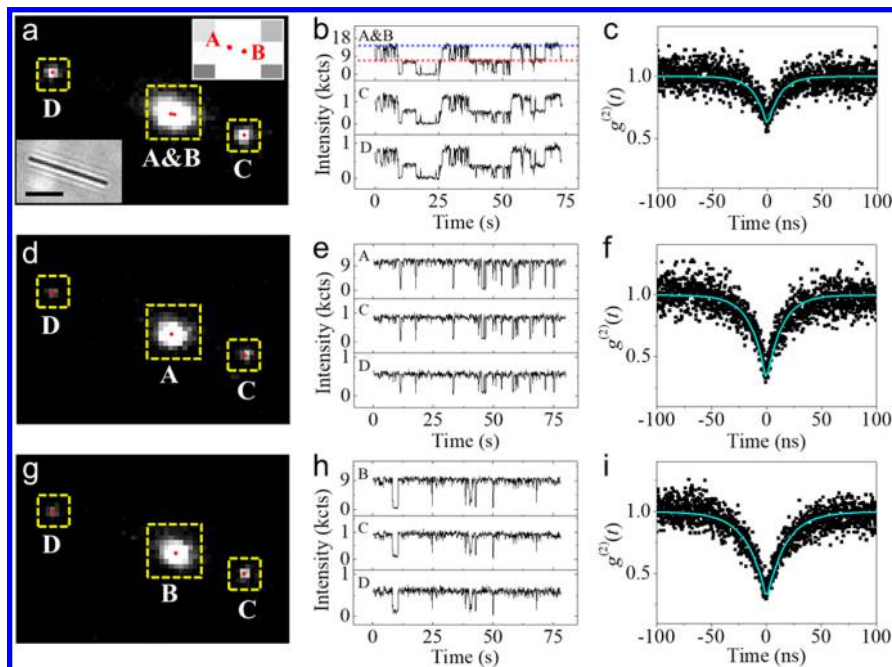

Figure 4. Selective excitation of two QDs separated by a distance smaller than the diffraction limit. (a) Fluorescence image of two nearby QDs A and B coupled to a Ag NW under the excitation of the SP standing wave generated by two laser beams at the NW ends C and D. The measured positions of QDs and the NW ends are labeled with red dots. The inset at the top right corner is an enlarged view of the spot A&B. The inset at the lower left corner shows the optical transmission image of the Ag NW. The scale bar corresponds to a length of 3 μm. The yellow squares denote the pixels used to track the emission intensities. (b) Time traces of the emission intensities from the spots A&B, C, and D recorded at a rate of 10 frames per second. The red and blue dash lines indicate the two bright states, which correspond to the emission intensity of only one QD and both two QDs in the bright state, respectively. (c) Second-order correlation function $g^{(2)}(t)$ of the fluorescence signal from the QDs A and B. The cyan solid line represents an exponential fitting of the black dots. (d,g) Fluorescence images showing the selective excitation of QD A (d) and QD B (g). The measured positions of the QDs and the NW ends are labeled with red dots. (e,h) Time traces of fluorescence emissions of QD A (e) and QD B (h) and scattered light at the NW ends C and D. (f,i) Second-order correlation function $g^{(2)}(t)$ of the selectively excited QD A (f) and QD B (i).

intensity oscillation under different intensity ratio I_L/I_P is also plotted in Figure 2k. The measured results have reproduced the simulation prediction, which confirms that the observed oscillation of QD emission intensity is because of the interference of localized SPs and propagating SPs on the NW.

Then we studied the controllable excitation of multiple QDs by tuning the interference field of two counter-propagating SP waves. We focused two laser beams EXC I and EXC II on the two ends of a Ag NW (Figure 3a) to generate two counter-propagating SP waves. The simulated electric field intensity distribution of a 15 nm Al_2O_3 coated Ag NW on glass substrate excited by two Gaussian beams with a phase difference of zero (Figure 3b) shows that a plasmonic standing wave is formed along the NW. The standing wave is found to move along the

NW when the phase of one Gaussian beam is shifted (see Section 4 of Supporting Information), which indicates the possibility of controllably exciting multiple QDs along the NW by changing the relative phase of the two incident laser beams.

This idea was tested experimentally using a Ag NW coupled with multiple QDs. The fluorescence image of the QDs-NW system under the wide-field excitation (Figure 3c) reveals five emission spots along the NW. Spots A and B correspond to two well separated QDs A and B. The spot C&D is from two nearby QDs C and D, which is evident by the time trace of emission intensity with two-level bright states (see Section 5 of Supporting Information). Spots E and F correspond to the two ends of the NW, where the propagating SPs generated by the QDs are scattered. Figure 3d shows the emission intensities of the four QDs excited by focusing the laser beams EXC I and EXC II onto the two ends of the NW E and F, respectively, with the phase of laser beam EXC I monotonically increased. Because of the close proximity of QDs C and D, their far field emissions have an overlap region. The emission intensities of the QDs C and D were recorded at the pixels marked by a green and a blue square (inset in Figure 3c), respectively, where the emissions did not overlap. The emission intensities of the QDs exhibit distinct phase dependent oscillations with different peak positions, which can be attributed to the varying near-field intensity on the NW during the moving of the standing wave. The phase difference between the peaks of different QDs can be used to determine the wavelength of the propagating SPs. In particular for the QDs C and D, the phase difference between the emission intensity peaks was determined to be 1.04π, which means that the two QDs have been selectively excited by tuning the phase difference of the two laser beams. The distance between the two QDs can be expressed as $L_{CD} = (2n + 1.04)/4 \cdot \lambda_{SP}$, where n is an integer and λ_{SP} is the wavelength of the propagating SPs. L_{CD} can be obtained by determining the central positions of the two QDs using the maximum likelihood single molecule localization method (see Section 6 of Supporting Information).[49−51] The fitted central positions of the two QDs are shown as red dots in the inset of Figure 3c, and a distance of 248 ± 10 nm between the two QDs is obtained. This results in the SP wavelength of $\lambda_{SP} = 326 \pm 13$ nm if $n = 1$ is chosen, which is quite close to the simulation result of 333 nm (Figure 3b). The excellent agreement between the experimentally extracted SP wavelength and the simulated SP wavelength confirms that the modulation of the emission intensities of the QDs is caused by the shifting of plasmonic standing wave along the NW.

As the minimum separation distance between the adjacent maximum and minimum electric field intensity is $\lambda_{SP}/4$, it is clear that for the NW in Figure 3b, two QDs with a separation of 83 nm can be selectively excited with the maximal ratio of the emission intensity of the two QDs. The resolution can be higher by setting a threshold smaller than the maximal emission intensity ratio. In order to test this resolution experimentally, we aimed to selectively excite two QDs with separation distance much smaller than the diffraction limit. Figure 4a shows the fluorescence image of two nearby QDs (QDs A and B) excited by the SP standing wave formed by the interference of two counter-propagating SP waves. The largest bright spot corresponds to the fluorescence emission of the excited QDs. The time trace of emission intensity from the yellow square A&B shows a blinking behavior with two bright states of intensity 7200 counts and 14800 counts (indicated by the red and blue dash lines in Figure 4b), corresponding to the

emission intensity of only one QD or both two QDs in the bright state, respectively. In order to confirm the existence of two QDs, we also measured the second-order correlation function $g^{(2)}(t)$ of the fluorescence from the QDs by using a Hanbury Brown-Twiss setup.[52] The resulting normalized antibunching curve (Figure 4c) verifies that the number of QDs in the detection area is two (see Section 7 of Supporting Information). The time traces of the scattered light at the NW ends C and D are correlated with that of the QD pair, which means that both the two QDs efficiently excited the propagating SPs on the Ag NW (see Section 8 of Supporting Information). The accurate positions of the two QDs are obtained using the single molecule localization method, and they are indicated with red dots in the inset of Figure 4a. The distance between the two QDs is determined to be 105 nm.

Then we moved the interference fringes of the standing wave by changing the relative phase of the two incident beams to selectively excite QD A or QD B. Figure 4d,g shows the fluorescence images when QD A and B are selectively excited, respectively. The accurate positions of the two QDs are obtained and labeled with red dots. The separation between the two QDs is about 100 ± 10 nm, which agrees well with the result obtained from Figure 4a. The selective excitation of each QD is confirmed by both the binary blinking in the time traces of the emission intensity (Figure 4e,h) and the antibunching curves of $g^{(2)}(0) < 0.5$ (Figure 4f,i). These results demonstrate that we have achieved the selective excitation of two QDs separated by a distance below the diffraction limit by tuning the interference pattern of the propagating SPs on the NW.

The tunable SP interference pattern on the plasmonic NW can also be applied to structured illumination microscopy (SIM) technique for a new kind of super-resolution imaging method. With the conventional SIM, the sample is illuminated by a series of sinusoidal excitation light patterns with different phase, which encodes the normally inaccessible high spatial frequency information on the sample into several recorded images. The obtained images are then processed to yield a final reconstruction with up to twice the normal resolution of the conventional microscopy.[53] Because the plasmonic standing wave along the metal NW provides one-dimensional longitudinally translated sinusoidal illuminations with higher spatial frequency than any possible fringes formed in the surrounding medium, the SIM performed on the plasmonic NW possesses superior resolving power compared with the conventional SIM.

Figure 5a shows the point spread function (PSF) of the conventional fluorescence microscopy. On the basis of the fluorescence images of single QDs in our experiment, the full width at half-maximum (fwhm) of the PSF is set to be 260 nm. In the simulation, we first used a single QD with diameter of 5 nm to obtain the PSF of the SIM performed on the Ag NW. The plasmonic standing wave shown in Figure 3b served as the structured illumination to excite the QD near the NW. A sequence of three images taken under illumination with initial phase difference of 0, $2\pi/3$, and $4\pi/3$ were used to extract the high spatial frequency information. The numerical algorithm of reconstructing the high-resolution image from the intermediate images is the same as that of the conventional SIM.[54−56] Figure 5b shows the obtained PSF of the single QD near the Ag NW using SIM method. Because the Fourier space is extended only in one direction, the PSF appears long and narrow. The fwhm of the PSF along the NW direction is 98 nm (Figure 5c), which indicates about 2.65 times resolution improvement compared with the conventional fluorescence microscopy. The simulation
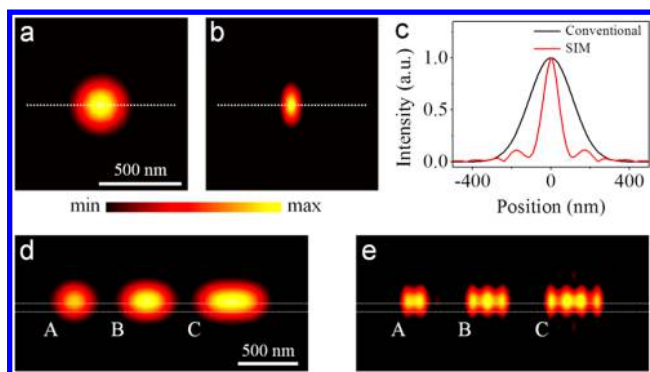
Figure 5. Super-resolution imaging of multiple QDs near a Ag NW using SIM method. (a) PSF of conventional fluorescence microscopy. (b) Reconstructed PSF of a single QD near the Ag NW using SIM method. (c) Intensity distribution of the PSF along the white dashed lines marked in (a) and (b). (d) Conventional fluorescence image of nine QDs along the Ag NW surface. The three bright spots A, B, and C correspond to the emission of two QDs separated by 96 nm, three QDs separated by 113 nm, and four QDs separated by 124 nm, respectively. The two white lines mark the position of the Ag NW. (e) Reconstructed super-resolution fluorescence image of the nine QDs along the NW using SIM method.

is also repeated for multiple QDs positioned along the NW to further illustrate the imaging performance of SIM on Ag NW. Figure 5d shows the conventional fluorescence image of nine QDs along the NW. The minimum separation distance between these QDs is only 96 nm. Because of the diffraction limit, we cannot identify the number of QDs in each bright spot. The reconstructed image (Figure 5e) shows a drastic resolution improvement, where the QDs in the diffraction limited area have been clearly resolved. This new SIM method is especially suitable for studying the system composed of a plasmonic waveguide and quantum emitters with temporally stabilized fluorescence, such as color centers in nanodiamonds, a promising element for quantum optics,[57] spin-based quantum information processing,[58] and high-resolution sensing.[59]

For controlling the excitation of QDs using SP interference, because the SP standing wave possesses symmetric electric field intensity distribution across the NW, the QDs symmetrically distributed on opposite sides of the NW always experience the same excitation condition and only QDs with a displacement along the NW direction can be selectively excited. The zigzag-shaped near-field intensity distribution induced by the interference of propagating SPs and localized SPs provides another kind of excitation scheme, which can selectively excite the QDs symmetrically distributed on the opposite sides of the NW. The two kinds of interference patterns provide different choices for the different QD position arrangements around the NW, which enhances the flexibility of this super-resolution selective excitation method (see Section 9 of Supporting Information). It is also feasible to excite localized SPs at multiple sites to interfere with the propagating SPs and superpose localized SPs onto the plasmonic standing wave to generate more complex interference patterns to realize particular excitation aims.

A powerful feature of this coupled system of multiple quantum emitters and plasmonic NW is that all the quantum emitters near the NW can be controllably excited, and their spontaneous emission can be strongly coupled to the quantized single SPs on the NW. It provides a suitable system to study the quantum interference of single SPs generated from two

quantum emitters. The plasmonic NW with tunable SP interference field would also be useful for optical imaging and sensing in chemical and biological systems with high spatial resolution and low background noise. Furthermore, by replacing the multiple quantum emitters near the NW with branch NWs, the propagating SPs on the branch NWs can be selectively launched by moving the SP interference fringes along the main NW, which provides a new method for SP routing in plasmonic nanocircuits.

In conclusion, we show that multiple QDs coupled with the plasmonic NW can be controllably excited by tuning the interference pattern of SPs on the NW. The superposition of localized SPs and propagating SPs forms a zigzag-shaped near-field distribution at the overlap region of these two modes, and the interference of two counter-propagating SP waves generates a standing wave pattern on the NW. By changing the relative phase of the two excitation beams, the interference patterns can be shifted along the NW, enabling the controllable excitation of multiple QDs on the NW. Using this technique, the selective excitation of two QDs with a separation of about 100 nm is demonstrated in experiment. Finally, we numerically demonstrate a new kind of super-resolution imaging method which combines the structured illumination microscopy technique with the tunable SP interference pattern on the NW. Our findings form the basis for a new kind of optical excitation and characterization technique breaking the diffraction limit, which can be extended to other kinds of plasmonic waveguide systems and benefit the studies of multiple quantum emitters coupled with plasmonic nanowaveguides and nanocircuits.

■ ASSOCIATED CONTENT

ⓢ Supporting Information

The Supporting Information is available free of charge on the ACS Publications website at DOI: 10.1021/acs.nanolett.7b05448.

> Details about the sample preparation and optical measurements, the direct and remote excitation of QDs near a Ag NW, the simulation of the visibility of the SP interference, the shift of the SP standing wave along the NW, the time trace of the emission intensity from a pair of QDs coupled with a Ag NW, the measurement of the distance between two QDs, the analysis of QDs number in the detection area, the calculation of SP-generation efficiency, two kinds of selective excitation scheme, and Figures S1–S10 (PDF)

■ AUTHOR INFORMATION

Corresponding Author

*E-mail: weihong@iphy.ac.cn.

ORCID ⓞ

Hong Wei: 0000-0002-3616-0386

Hongxing Xu: 0000-0002-1718-8834

Notes

The authors declare no competing financial interest.

■ ACKNOWLEDGMENTS

■ REFERENCES

(1) Bennett, C. H.; Brassard, G. *Theor. Comput. Sci.* **2014**, *560*, 7−11.

(2) Kimble, H. J. *Nature* **2008**, *453*, 1023−1030.

(3) Kok, P.; Munro, W. J.; Nemoto, K.; Ralph, T. C.; Dowling, J. P.; Milburn, G. J. *Rev. Mod. Phys.* **2007**, *79*, 135−174.

(4) Novotny, L.; van Hulst, N. *Nat. Photonics* **2011**, *5*, 83−90.

(5) Pelton, M. *Nat. Photonics* **2015**, *9*, 427−435.

(6) Anger, P.; Bharadwaj, P.; Novotny, L. *Phys. Rev. Lett.* **2006**, *96*, 113002.

(7) Kühn, S.; Håkanson, U.; Rogobete, L.; Sandoghdar, V. *Phys. Rev. Lett.* **2006**, *97*, 017402.

(8) Kinkhabwala, A.; Yu, Z. F.; Fan, S. H.; Avlasevich, Y.; Mullen, K.; Moerner, W. E. *Nat. Photonics* **2009**, *3*, 654−657.

(9) Ureña, E. B.; Kreuzer, M. P.; Itzhakov, S.; Rigneault, H.; Quidant, R.; Oron, D.; Wenger, J. *Adv. Mater.* **2012**, *24*, OP314.

(10) Curto, A. G.; Volpe, G.; Taminiau, T. H.; Kreuzer, M. P.; Quidant, R.; Van Hulst, N. F. *Science* **2010**, *329*, 930−933.

(11) Aouani, H.; Mahboub, O.; Devaux, E.; Rigneault, H.; Ebbesen, T. W.; Wenger, J. *Nano Lett.* **2011**, *11*, 2400−2406.

(12) Ditlbacher, H.; Hohenau, A.; Wagner, D.; Kreibig, U.; Rogers, M.; Hofer, F.; Aussenegg, F. R.; Krenn, J. R. *Phys. Rev. Lett.* **2005**, *95*, 257403.

(13) Nauert, S.; Paul, A.; Zhen, Y. R.; Solis, D.; Vigderman, L.; Chang, W. S.; Zubarev, E. R.; Nordlander, P.; Link, S. *ACS Nano* **2014**, *8*, 572−580.

(14) Wei, H.; Pan, D.; Zhang, S. P.; Li, Z. P.; Li, Q.; Liu, N.; Wang, W. H.; Xu, H. X. *Chem. Rev.* http://dx.doi.org/10.1021/acs.chemrev.7b00441.

(15) Chang, D. E.; Sorensen, A. S.; Hemmer, P. R.; Lukin, M. D. *Phys. Rev. Lett.* **2006**, *97*, 053002.

(16) Fedutik, Y.; Temnov, V. V.; Schops, O.; Woggon, U.; Artemyev, M. V. *Phys. Rev. Lett.* **2007**, *99*, 136802.

(17) Wei, H.; Ratchford, D.; Li, X. Q.; Xu, H. X.; Shih, C. K. *Nano Lett.* **2009**, *9*, 4168−4171.

(18) Pyayt, A. L.; Wiley, B.; Xia, Y. N.; Chen, A.; Dalton, L. *Nat. Nanotechnol.* **2008**, *3*, 660−665.

(19) Guo, X.; Qiu, M.; Bao, J. M.; Wiley, B. J.; Yang, Q.; Zhang, X. N.; Ma, Y. G.; Yu, H. K.; Tong, L. M. *Nano Lett.* **2009**, *9*, 4515−4519.

(20) Wei, H.; Wang, Z. X.; Tian, X. R.; Kall, M.; Xu, H. X. *Nat. Commun.* **2011**, *2*, 387.

(21) Wei, H.; Xu, H. X. *Nanophotonics* **2012**, *1*, 155−169.

(22) Akimov, A. V.; Mukherjee, A.; Yu, C. L.; Chang, D. E.; Zibrov, A. S.; Hemmer, P. R.; Park, H.; Lukin, M. D. *Nature* **2007**, *450*, 402−406.

(23) Kolesov, R.; Grotz, B.; Balasubramanian, G.; Stöhr, R. J.; Nicolet, A. A. L.; Hemmer, P. R.; Jelezko, F.; Wrachtrup, J. *Nat. Phys.* **2009**, *5*, 470−474.

(24) Huck, A.; Kumar, S.; Shakoor, A.; Andersen, U. L. *Phys. Rev. Lett.* **2011**, *106*, 096801.

(25) Chang, D. E.; Sørensen, A. S.; Demler, E. A.; Lukin, M. D. *Nat. Phys.* **2007**, *3*, 807−812.

(26) Kumar, S.; Huck, A.; Andersen, U. L. *Nano Lett.* **2013**, *13*, 1221−1225.

(27) Li, Q.; Wei, H.; Xu, H. X. *Nano Lett.* **2015**, *15*, 8181−8187.

(28) Cai, T.; Dutta, S.; Aghaeimeibodi, S.; Yang, Z.; Nah, S.; Fourkas, J. T.; Waks, E. *Nano Lett.* **2017**, *17*, 6564−6568.

(29) Kim, N. C.; Li, J. B.; Yang, Z. J.; Hao, Z. H.; Wang, Q. Q. *Appl. Phys. Lett.* **2010**, *97*, 061110.

(30) Chen, G. Y.; Chen, Y. N. *Opt. Lett.* **2012**, *37*, 4023−4025.

(31) Kim, N. C.; Ko, M. C.; Wang, Q. Q. *Plasmonics* **2015**, *10*, 611−615.

(32) Martín-Cano, D.; Martín-Moreno, L.; García-Vidal, F. J.; Moreno, E. *Nano Lett.* **2010**, *10*, 3129−3134.

(33) Gonzalez-Tudela, A.; Martin-Cano, D.; Moreno, E.; Martin-Moreno, L.; Tejedor, C.; Garcia-Vidal, F. J. *Phys. Rev. Lett.* **2011**, *106*, 020501.

(34) Li, Q.; Wei, H.; Xu, H. X. *Nano Lett.* **2014**, *14*, 3358−3363.

(35) Gruber, A.; Drabenstedt, A.; Tietz, C.; Fleury, L.; Wrachtrup, J.; Von Borczyskowski, C. *Science* **1997**, *276*, 2012−2014.

(36) Gruber, C.; Trugler, A.; Hohenau, A.; Hohenester, U.; Krenn, J. R. *Nano Lett.* **2013**, *13*, 4257−4262.

(37) Tran, T. T.; Fang, J.; Zhang, H.; Rath, P.; Bray, K.; Sandstrom, R. G.; Shimoni, O.; Toth, M.; Aharonovich, I. *Adv. Mater.* **2015**, *27*, 4048−4053.

(38) Bermudez-Urena, E.; Gonzalez-Ballestero, C.; Geiselmann, M.; Marty, R.; Radko, I. P.; Holmgaard, T.; Alaverdyan, Y.; Moreno, E.; Garcia-Vidal, F. J.; Bozhevolnyi, S. I.; Quidant, R. *Nat. Commun.* **2015**, *6*, 7883.

(39) Hell, S. W.; Wichmann, J. *Opt. Lett.* **1994**, *19*, 780−782.

(40) Klar, T. A.; Jakobs, S.; Dyba, M.; Egner, A.; Hell, S. W. *Proc. Natl. Acad. Sci. U. S. A.* **2000**, *97*, 8206−8210.

(41) Arroyo-Camejo, S.; Adam, M. P.; Besbes, M.; Hugonin, J. P.; Jacques, V.; Greffet, J. J.; Roch, J. F.; Hell, S. W.; Treussart, F. *ACS Nano* **2013**, *7*, 10912−10919.

(42) Neumann, L.; Pang, Y.; Houyou, A.; Juan, M. L.; Gordon, R.; van Hulst, N. F. *Nano Lett.* **2011**, *11*, 355−360.

(43) Mivelle, M.; van Zanten, T. S.; Garcia-Parajo, M. F. *Nano Lett.* **2014**, *14*, 4895−4900.

(44) Li, Z. P.; Bao, K.; Fang, Y. R.; Huang, Y. Z.; Nordlander, P.; Xu, H. X. *Nano Lett.* **2010**, *10*, 1831−1835.

(45) Wang, L. L.; Zou, C. L.; Ren, X. F.; Liu, A. P.; Lv, L.; Cai, Y. J.; Sun, F. W.; Guo, G. C.; Guo, G. P. *Appl. Phys. Lett.* **2011**, *99*, 061103.

(46) Li, Q.; Wei, H.; Xu, H. X. *Chin. Phys. B* **2014**, *23*, 097302.

(47) Galland, C.; Ghosh, Y.; Steinbruck, A.; Sykora, M.; Hollingsworth, J. A.; Klimov, V. I.; Htoon, H. *Nature* **2011**, *479*, 203−207.

(48) Johnson, P. B.; Christy, R. W. *Phys. Rev. B* **1972**, *6*, 4370−4379.

(49) Stranahan, S. M.; Willets, K. A. *Nano Lett.* **2010**, *10*, 3777−3784.

(50) Cang, H.; Labno, A.; Lu, C. G.; Yin, X. B.; Liu, M.; Gladden, C.; Liu, Y. M.; Zhang, X. *Nature* **2011**, *469*, 385−388.

(51) Smith, C. S.; Joseph, N.; Rieger, B.; Lidke, K. A. *Nat. Methods* **2010**, *7*, 373−375.

(52) Hanbury Brown, R.; Twiss, R. Q. *Nature* **1956**, *177*, 27−29.

(53) Gustafsson, G. L. *J. Microsc.* **2000**, *198*, 82−87.

(54) Frohn, J. T.; Knapp, H. F.; Stemmer, A. *Proc. Natl. Acad. Sci. U. S. A.* **2000**, *97*, 7232−7236.

(55) Gustafsson, G. L. *Proc. Natl. Acad. Sci. U. S. A.* **2005**, *102*, 13081−13086.

(56) Wei, F. F.; Liu, Z. W. *Nano Lett.* **2010**, *10*, 2531−2536.

(57) Babinec, T. M.; Hausmann, B. J. M.; Khan, M.; Zhang, Y.; Maze, J. R.; Hemmer, P. R.; Loncar, M. *Nat. Nanotechnol.* **2010**, *5*, 195−199.

(58) Fuchs, G. D.; Burkard, G.; Klimov, P. V.; Awschalom, D. D. *Nat. Phys.* **2011**, *7*, 789−793.

(59) Balasubramanian, G.; Chan, I. Y.; Kolesov, R.; Al-Hmoud, M.; Tisler, J.; Shin, C.; Kim, C.; Wojcik, A.; Hemmer, P. R.; Krueger, A.; Hanke, T.; Leitenstorfer, A.; Bratschitsch, R.; Jelezko, F.; Wrachtrup, J. *Nature* **2008**, *455*, 648−651.